SCIENTIFIC REPORTS

OPEN

SUBJECT AREAS:
HETEROGENEOUS CATALYSIS
MOLECULAR SELF-ASSEMBLY

Received
21 November 2013

Accepted
5 February 2014

Published
1 April 2014

Correspondence and requests for materials should be addressed to Y.Y. (catalyticscience@163.com)

New route toward building active ruthenium nanoparticles on ordered mesoporous carbons with extremely high stability

Ying Yang[1], Chengjun Sun[2], Yang Ren[2], Shijie Hao[1] & Daqiang Jiang[1]

[1]State Key Laboratory of Heavy Oil Processing, China University of Petroleum, Changping, Beijing 102249, China, [2]X-ray Science Division, Argonne National Laboratory, 9700 S. Cass Ave., Argonne, Illinois 60439, USA.

Creating highly active and stable metal catalysts is a persistent goal in the field of heterogeneous catalysis. However, a real catalyst can rarely achieve both of these qualities simultaneously due to limitations in the design of the active site and support. One method to circumvent this problem is to fabricate firmly attached metal species onto the voids of a mesoporous support formed simultaneously. In this study, we developed a new type of ruthenium catalyst that was firmly confined by ordered mesoporous carbons through the fabrication of a cubic *Ia3d* chitosan-ruthenium-silica mesophase before pyrolysis and silica removal. This facile method generates fine ruthenium nanoparticles (*ca.* 1.7 nm) that are homogeneously dispersed on a mesoporous carbonaceous framework. This ruthenium catalyst can be recycled 22 times without any loss of reactivity, showing the highest stability of any metal catalysts; this catalyst displays a high activity (23.3 $mol_{LA}h^{-1}g_{metal}^{-1}$) during the catalytic hydrogenation of levulinic acid (LA) when the metal loading is 6.1 wt%. Even at an ultralow loading (0.3 wt%), this catalyst still outperforms the most active known Ru/C catalyst. This work reveals new possibilities for designing and fabricating highly stable and active metal catalysts by creating metal sites and mesoporous supports simultaneously.

Supported ruthenium catalysts are highly efficient in various reactions, such as ammonia synthesis, Fischer-Tropsh synthesis, selective hydrogenation and cellulose hydrolysis[1–7]. Ordered mesoporous carbon supported ruthenium (Ru-OMC) catalysts are highly favourable due to the combined advantages of the active ruthenium species and a unique OMC support with well controlled porosity and structures, as well as superior acid-base tolerance and (hydro)thermal stability[8,9]. However, the Ru-OMC catalysts usually exhibit poor stability due to their property toward aggregation and severe leaching of the ruthenium species[10–12], caused by their poor dispersion and weak interfacial contact with the OMC. The Ru-OMC catalysts are usually fabricated using traditional impregnation or precipitation techniques after synthesising the OMC *via* a hard-templating approach[13]. This tedious multi-step synthesis exerts poor control over the ruthenium dispersion and its attachment onto OMC. Such dilemma is relieved by filling the ordered mesoporous SBA-15 with carbon and metal precursors before pyrolysis and silica removal[14,15]. Currently, an alternative and more economic approach can deposit homogeneously dispersed metal nanoparticles (NPs) firmly attached to a carbonaceous framework formed simultaneously *in situ* by the direct pyrolysis of metal organic frameworks (MOFs) under an inert atmosphere[16,17]. However, the resulting carbonaceous frameworks are disordered and lack uniform mesoporous arrays due to the uncontrolled transformation of flexible MOFs during pyrolysis. To date, fabricating highly stable Ru-OMC catalysts with ruthenium species homogeneously dispersed on ordered mesoporous carbons using a facile method remains a challenge.

The direct pyrolysis of a metal-free ordered mesophase involving a surfactant-directed polycondensation of resorcinol and formaldehyde can afford OMC[18]. Therefore, if ruthenium precursors could be introduced to this reaction mixture, a Ru-OMC catalyst with firmly anchored Ru NPs homogeneously dispersed on OMC might be prepared *in situ*. A chelated polymerisable carbon precursor is crucialfor the oriented synthesis of an ordered mesophase containing homogeneously distributed ruthenium coordination polymers. Chitosan is a naturally occurring macromolecule that possesses numerous hydroxyl and amine moieties with a strong affinity for metal

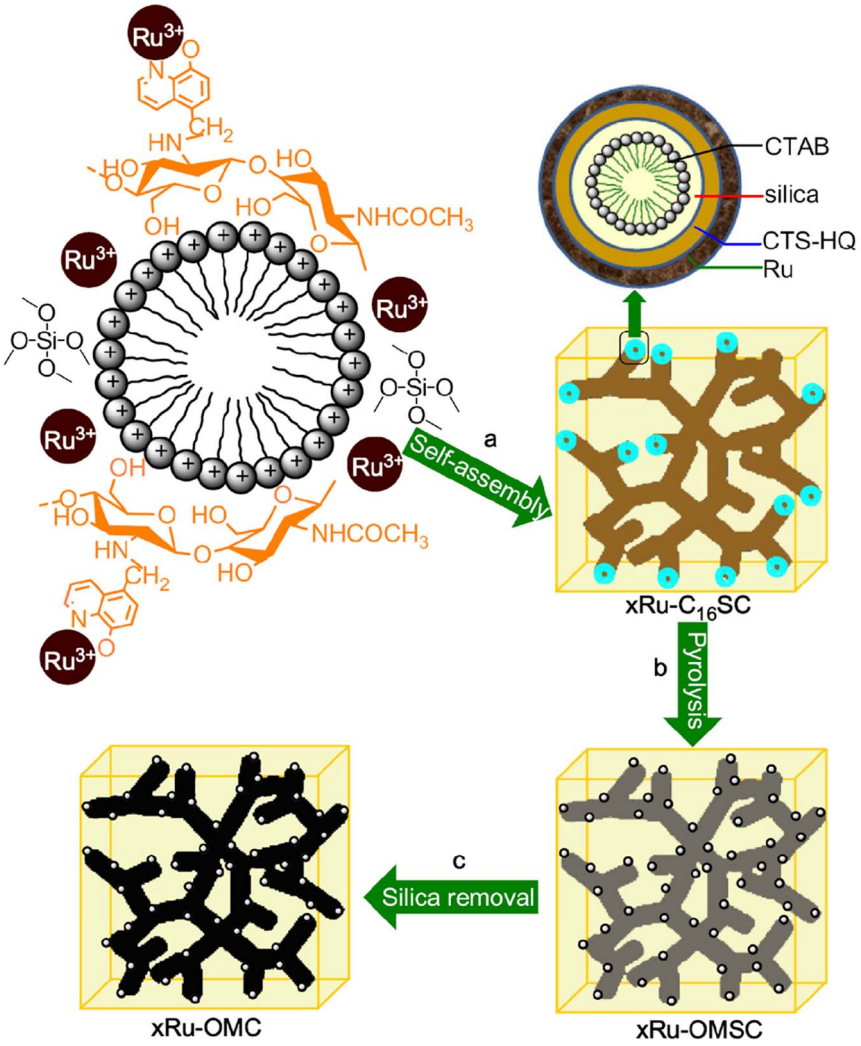

Figure 1 | Synthetic strategy for the Ru-OMC catalysts. The construction of a cubic *Ia3d* chitosan-ruthenium-silica mesophase *via* CTAB-directed self-assembly of CTS-HQ, TMOS and $RuCl_3 \cdot 3H_2O$ under basic conditions was carried out before pyrolysis and silica removal.

ions[19]. Therefore, chitosan may be superior to the phenolic resin extensively used as the chelating agent for dispersing metal species and interacting with the surfactant to form an ordered mesophase.

We introduce a new type of highly stable and active Ru-OMC catalyst fabricated *in situ* by constructing a CTAB-directed cubic *Ia3d*chitosan-ruthenium-silica mesophase before pyrolysis and silica removal. In our study, the chitosan (CTS) was initially modified by 5-chloromethyl-8-quinolinol (Supplementary Information and Supplementary Figs. S1–6), facilitating chelation with the ruthenium ions and interaction with positive CTA^+ to enlarge the hydrophobic volume of the surfactant; these changes decrease the micelle curvature to form a cubic *Ia3d* mesophase along with the silica (Supplementary Information). This chitosan-ruthenium-silica mesophase provides an interpenetrating framework with a "reinforced-concrete"-like structure; both "reinforcing-steel-bar" silicate and "concrete" carbons form the mesostructured framework (Supplementary Fig. S7). The pyrolysis is a unique "one stone, three birds" strategy used to remove the CTAB, carbonise the CTS and reduce the ruthenium ions in one step. The silica framework acts as a hard template to consolidate the cubic *Ia3d* structure during pyrolysis, and removing the silica affords replicated intercrossed carbonaceous mesopores with large surface areas and pore volumes; the Ru NPs are also exposed. By using this facile fabrication methodology, fine Ru NPs (*ca.* 1.7 nm) were confined and homogeneously dispersed on the ordered mesoporous carbonaceous framework. This Ru-OMC catalyst can be recycled 22 times without any apparent loss of reactivity, demonstrating the highest stability of any metal catalyst and a high activity (23.3 $mol_{LA}h^{-1}g_{metal}^{-1}$) for the catalytic hydrogenation of levulinic acid (LA) when the metal loading is 6.1 wt%. When used at an ultralow loading (0.3 wt%), this catalyst still outperforms the most active known Ru/C catalyst.

Results

Synthesis. Surfactant cetyltrimethylammonium bromide (CTAB), tetramethoxysilane (TMOS), 8-quinolinol modified chitosan (CTS-HQ) and ruthenium trichloridetrihydrate ($RuCl_3 \cdot 3H_2O$) were the structure directing agent, silica, carbon and metal precursors used to synthesise Ru-OMC catalysts, respectively. The molar proportion of the precursor gel was as follows: 0.15 CTAB: 8.2 NH_3 (25 wt%): 114 H_2O: 10 EtOH: 0.9 TEOS: 0.5 CTS-HQ: 2xRu, where x was set as 0, 0.001, 0.005, 0.015, 0.030 and 0.060. After the mixture was stirred at room temperature for 2 h, the resulting gel was transferred to a polytetrafluoroethylene container and heated at 100°C for 2 days (Fig. 1a). The as-made product (xRu-C_{16}SC) was washed, dried and pyrolysed in a tubular furnace under N_2. The heating rate was 2°C/min below 350°C and 5°C/min above 350°C; the pyrolysis was carried out at 750°C for 2 h (Fig. 1b). The resulting solid with different metal contents was denoted as xRu-OMSC and subjected

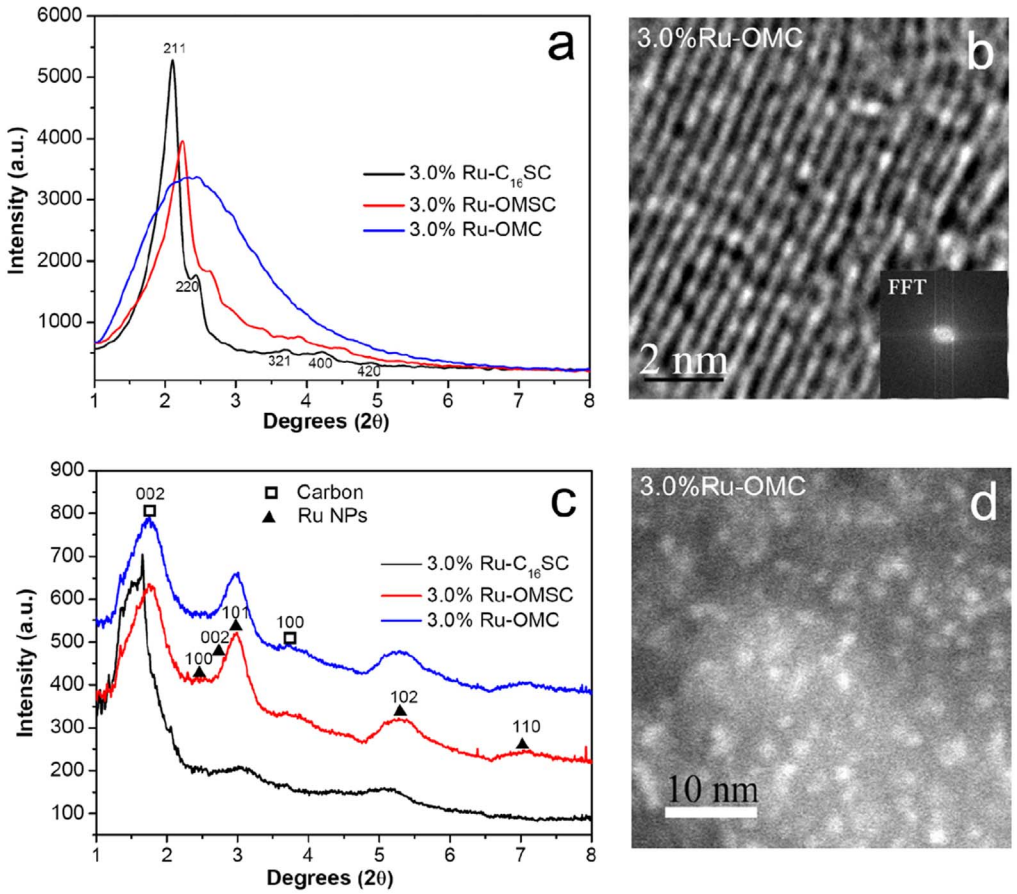

Figure 2 | Characterisation results for the Ru-containing samples. (a) Small angle X-ray diffraction patterns of 3.0%Ru-C_{16}SC, 3.0%Ru-OMSC and 3.0%Ru-OMC, (b) TEM image with the corresponding FFT pattern of 3.0%Ru-OMC, (c) high-energy X-ray diffraction patterns of 3.0%Ru-C_{16}SC, 3.0%Ru-OMSC and 3.0%Ru-OMC, and (d) the HAADF image of 3.0%Ru-OMC.

to alkaline etching with 0.5 M NaOH solution to remove any silica layers, affording xRu-OMC (Fig. 1c).

Characterisation. The small angle X-ray diffraction patterns of 3.0%Ru-C_{16}SC and 3.0%Ru-OMSC show cubic *Ia3d* featured (211), (220), (321), (400) and (420) diffractions in a 2θ range from 2 to 5° (Fig. 2a), corresponding to the long-range ordered 3D mesostructure[20,21]. However this structure shrinks slightly upon silica removal, as suggested by the broadening (211) peak. This ordered mesostructured array is further confirmed by bright-field TEM imaging (Fig. 2b). The pyrolysed and alkaline-etched samples provide broad but clear (101), (102) and (110) diffractions (Fig. 2c) that correspond to *hcp* structured Ru NPs (JCPDS file 06-0663)[22]. These Ru NPs can be directly discerned in the high-angle annular dark-field (HAADF) image of 3.0%Ru-OMC; this material exhibits homogeneously dispersed bright spots centred at *ca.* 1.7 nm (Fig. 2d). Interestingly, the average particle size of the Ru NPs remains invariably at approximately 1.7 nm when the ruthenium concentration varies; just the dispersion of uniformly distributed Ru NPs improves as the molar percentage of Ru decreases (Supplementary Fig. S8).

The X-ray absorption fine structure (XAFS) reveals the transition and local structure of ruthenium species. Compared to 3.0%Ru-C_{16}SC, 3.0%Ru-OMSC exhibits a pre-edge feature and a negative shift in the adsorption edge position (Fig. 3a), suggesting that the Ru(+3) species are mostly reduced during pyrolysis[23,24]. After alkaline etching, 3.0%Ru-OMC provides unexpected X-ray absorption near edge structure (XANES), as well as k^2-weighted extended X-ray absorption fine structure (EXAFS) spectra similar to those of 3.0%Ru-C_{16}SC; the weak oscillations at a higher k region of $k > 8$ Å^{-1} (Supplementary Fig. S9) indicate the dominance of low Z backscatter, corresponding to O in our system[25]. Moreover, 3.0%Ru-OMC shows one prominent peak at 1.60 Å from the Ru-O pairs in the Fourier transformed EXAFS (r space), in addition to the peak at 2.20 Å from the Ru-Ru contributions[26] (Fig. 3b). Consistently, preliminary data analysis indicates that the 3.0%Ru-OMC exhibits fewer Ru-Ru contributions (curve fitted to be 2.70 Å) with a smaller coordination number of ~1.8 compared to that of ~4.9 from 3.0%Ru-OMSC and is accompanied by the Ru-O contributions with a coordination number of ~3.3, suggesting that the Ru NPs were partially oxidised during the alkaline etching[27]. Detailed EXAFS data analysis is presented in Table 1.

The incorporation of CTS-HQ and silica into the CTAB-directed chitosan-ruthenium-silica mesophase can be confirmed by the C-H stretching vibration at 2927 and 2855 cm^{-1}, the pyridyl and aromatic ring vibrations between 1600 and 1300 cm^{-1}, and the silica framework vibration at 1086 and 465 cm^{-1}[28–30] (Supplementary Fig. S10). After pyrolysis, only the silica vibrations persist; these vibrations disappear after the silica is removed, as verified by the absence of Si signals in the EDX spectrum compared to 3.0%Ru-OMSC (Supplementary Fig. S11). The transition of 3.0%Ru-C_{16}SC triggers a morphological change from a uniform sphere to a deficient hollow shape (Supplementary Fig. S12), and creates mesoporous 3.0%Ru-OMSC and 3.0%Ru-OMC with uniform pores which can be verified by the type IV isotherms and H_1-type hysteresis loops of the corresponding materials (see Fig. 3c). The pore size slightly increases (0.5%), while the specific surface area and pore volume increase dramatically after silica removal with values nearly three times higher

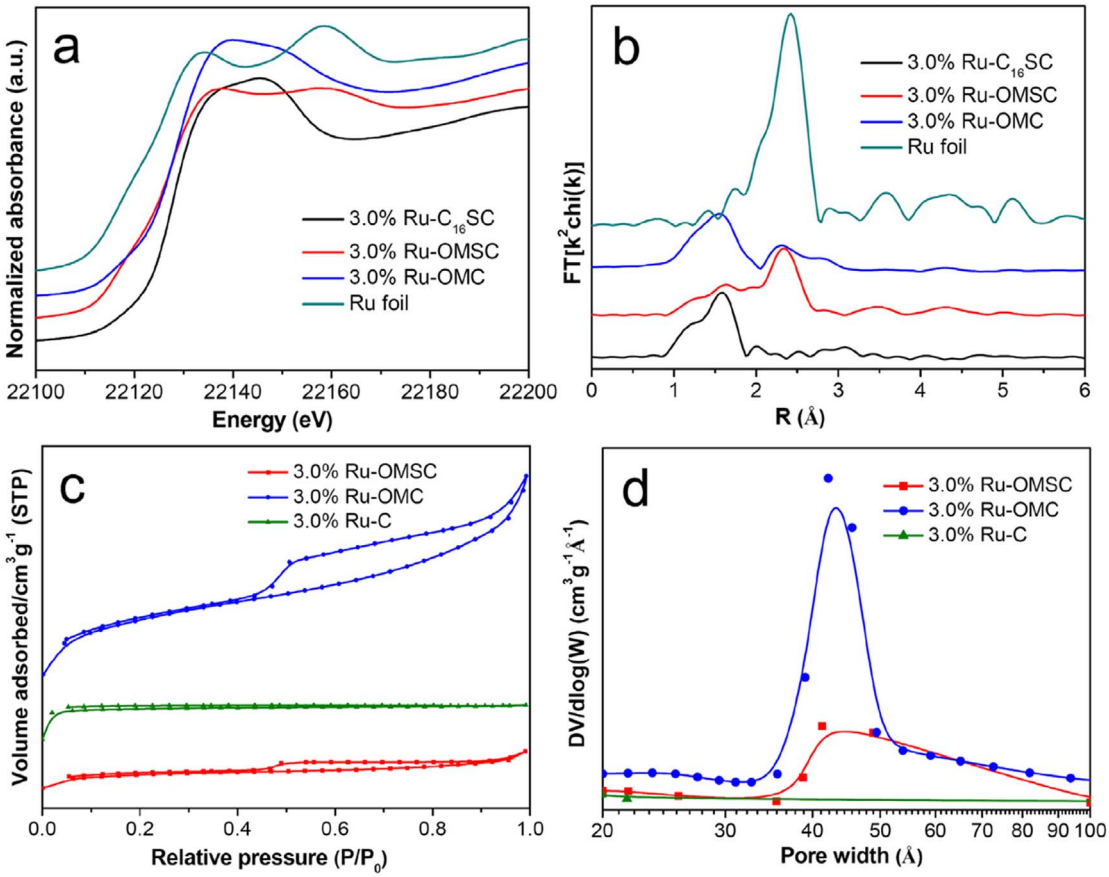

Figure 3 | Characterisation results for the Ru-containing samples. (a)The normalised XANES spectra at the Ru K-edge and (b) the k^2-weighted Fourier transform spectra from EXAFS for 3.0%Ru-C_{16}CS, 3.0%Ru-OMSC, 3.0%Ru-OMC and Ru foil. (c) N_2 adsorption/desorption isotherms and (d) the BJH pore size distributions of 3.0%Ru-OMSC, 3.0%Ru-OMC and 3.0%Ru-C.

than those of 3.0%Ru-OMSC (Fig. 3d and Supplementary Table S1). The S_{meso}/S_{micro}ratio and V_{meso}/V_{micro}ratio also increase from 0.72 to 0.88 and from 2.17 to 3.55 because more mesostructures are created after the silica is removed. Accordingly, the wall thickness is calculated by subtracting $D_p/2$ from $A_0/3.0919$[31], decreasing from 0.96 to 0.69 nm (Supplementary Table S1). Based on the above results, the Ru NP size (*ca.* 1.7 nm) ranges between the pore size (*ca.* 4.32 nm) and wall thickness (0.69 nm), revealing that the Ru NPs are primarily affixed to the mesoporous frameworks.

Catalytic performance. We chose typical levulinic acid (LA) hydrogenation to probe the catalytic performance of the xRu-OMC series, and commercial Ru/C isthe most active of the metal catalysts for this process. Supplementary Table S2 lists the catalytic results over 3.0%Ru-OMC under different reaction conditions. For the catalytic conversion of 5.0 g of LA under solvent-free conditions, a 99.4% LA conversion and a 98.8% yield of γ-valerolactone (GVL) are achieved when 3 wt% of catalyst was used under 4.5 MPa H_2 at 150°C for 2 h. The results for the other catalysts using these optimised reaction conditions are shown in Table 2. As expected, the OMC shows insignificant activity due to the lack of active ruthenium species. When increasing ruthenium content from 0.3 to 6.1 wt%, all of the Ru-OMC catalysts are active; the LA conversion and GVL yield increase dramatically. However, increasing the ruthenium loading from 6.1 to 12.6% decreases the LA conversion and GVL yield, most likely due to the poor dispersion of Ru NPs. In contrast, the specific rates and TOF values decrease when the ruthenium content increases, and 0.1%Ru-OMC exhibits the highest specific rate (34.7 $mol_{LA}h^{-1}g_{metal}^{-1}$) and TOF value (3510 h^{-1}) of any xRu-OMC catalyst, making it approximately three times more active than commercial Ru/C. These results suggest that the catalytic activity of Ru-OMC can be tuned by varying the ruthenium content.

The textural properties of the carbonaceous supports affect the catalytic performance of the supported Ru NPs. For comparison, microporous 3.0%Ru-C was prepared *via* the direct pyrolysis of

Table 1 | Best fit parameters obtained from the analysis of the Ru K-edge EXAFS spectra[a]

Materials	Shell	Fitting range Δr [Å]	CN	R [Å]	ΔE_0 [eV]	R factor (%)
3.0%Ru-OMSC	Ru-Ru	0.897–2.718	4.9 ± 1.0	2.65 ± 0.016	−5.9 ± 2.4	4.6
3.0%Ru-OMC	Ru-O	0.552–2.053	3.3 ± 0.2	2.01 ± 0.011	8.4 ± 1.2	0.9
	Ru-Ru	0.552–3.352	1.8 ± 0.2	2.70 ± 0.011	5.5 ± 1.4	-
Ru foil	Ru-Ru	-	12	2.67		-

[a]CN = coordination number, R = coordination distance and ΔE_0 = inner potential correction. Error bounds (accuracies) that characterize the structural parameters obtained by EXAFS spectroscopy were estimated as CN, ±20%; R, ±1%; ΔE_0, ±20%. Ru foil parameter from data_9008513-ICSD; RuO_2 parameter from data_1000058-ICSD; r space fit, Δk = 2.8–10.0 $Å^{-1}$, Δr = 0.5–3.3 Å, S_0^2 fitting from RuO_2 foil defined as 0.95.

Table 2 | Comparison of rates and TOFs

Materials	Ru loadings (wt%)	LA conversion[a] (%)	GVL yield (%)	Specific rate ($mol_{LA}h^{-1}g_{metal}^{-1}$)	TOF[b] (h^{-1})
OMC	0	3.4	-	-	-
0.1%Ru-OMC	0.3	7.8	6.6	34.7	3510
0.5%Ru-OMC	1.0	21.9	19.7	30.3	3061
1.5%Ru-OMC	3.7	72.1	65.9	28.0	2827
3.0%Ru-OMC	6.1	99.4	98.8	23.3	2351
6.0%Ru-OMC	12.6	97.4	96.9	11.1	1119
3.0%Ru-OMSC	4.8	39.2	36.4	11.9	1197
3.0%Ru-C	5.5	33.5	-	8.7	882
commercial Ru/C	5.0	48.3	30.3	13.9	1403

[a]Reaction conditions: LA 5.0 g, catalyst amount 0.3 wt%, H_2 pressure 4.5 MPa, temperature 150°C and duration 2 h.
[b]TOF, h^{-1}: (turnover frequency) moles of substrate converted per mole of metal per hour.

chitosan-ruthenium coordination polymers in the absence of CTAB and silica; this material converts 33.3% of LA without producing GVL. GVL formation and diffusion were most likely prohibited in this microporous catalyst system. The LA conversion was enhanced to 39.2% with 36.4% GVL yield over the mesoporous 3.0%Ru-OMSC. The LA conversion and GVL yield are further improved to 99.4 and 98.8% over the 3.0%Ru-OMC catalyst due to the larger surface areas and mesoporous volumes created after silica removal[32], facilitating LA adsorption and GVL diffusion.

The recycling stability of the metal catalysts is important for their potential applications in industry. In our experiment, the spent catalyst was subjected to simple washing and was used directly in the following cycle. In this case, the 3.0%Ru-OMC catalyst can be recycled up to 22 times without any loss of reactivity (Fig. 4a); an ICP analysis of the filtration shows insignificant ruthenium content, exhibiting the highest stability of any tested metal catalyst. In the HAADF image of the spent 3.0%Ru-OMC after 23 cycles, slightly agglomerated NPs were observed (Supplementary Fig. S13), which is mainly responsible for the decreased but still high GVL yield (90.2%). The high stability of the 3.0%Ru-OMC can be ascribed to the active Ru NPs being firmly attached to the carbonaceous framework with the strong metal support interaction[33], as well as the strong electrostatic repulsion between the surface RuO_x coated Ru NPs, decreasing agglomeration[34].

A general comparison of the activity and stability during the catalytic hydrogenation of LA over various metal catalysts is shown in Fig. 4b. Most metal catalysts exhibit either very low activity with higher stability, such as Ni/C, or suffer fast current deactivation, such as Ru/C. The Ru-OMC catalyst developed in this study simultaneously exhibits extremely high stability and activity, making it unique due to its catalytic properties compared to other metal catalysts.

Discussion

In this study, a highly stable and active Ru-OMC catalyst was developed by fabricating a cubic *Ia3d* chitosan-ruthenium-silica mesophase before pyrolysis and silica removal. This facile and scalable methodology created homogeneously dispersed fine Ru NPs firmly confined onto the ordered mesoporous carbonaceous framework formed simultaneously *in situ*. This material developed a high stability and activity due to the elaborately fabricated ruthenium species, the mesostructured carbonaceous framework and the faithful occurrence of their ensemble effect. Using the concept of creating metal sites and mesoporous supports simultaneously *in situ*, this work opens new avenues for designing and fabricating various heterogeneous mono-, bi- and/or tri-metallic catalysts with exceptional performance.

Methods

Catalytic test. The LA hydrogenation reactions were carried out in a 100 ml magnetometrically stirred Parr 4560 autoclave equipped with a P.I.D. controller (4843). In a typical procedure, a known amount of catalyst and 5.0 g of LA were inserted into the autoclave. The sealed autoclave was charged and deflated with N_2 three times before being pressurised with H_2 to a certain value and heated to the reaction temperature. Once the desired temperature was reached, the timer was started. After the reaction was finished, the autoclave was cooled rapidly with cold water. Afterward, toluene was added as an internal standard. The reaction products were quantified with an Agilent 6980 gas chromatograph equipped with a flame ionisation detector and an SE-54 capillary column (30 m × 0.25 mm × 1.5 μm).

Characterisation. Powder XRD data were collected with a Bruker D8 Advance X-ray diffractometer using nickel filtered CuKα radiation (λ = 1.5406 Å). The samples were scanned from 2θ = 1.2–10.0° in 2°/min steps. The morphology and microstructure were analysed using a FEI Tecnai G2 F20 transmission electron microscope equipped with an energy dispersive X-ray spectroscopic analyser at 200 kV. The samples were sonicated for 5 min in ethanol, and one drop of the suspended sample was dripped onto a holely carbon film supported on a 300 mesh copper grid. The N_2 adsorption/desorption isotherms were recorded at 77 K with a Micromeritics Tristar II 3020. Before the measurements, the samples were outgassed

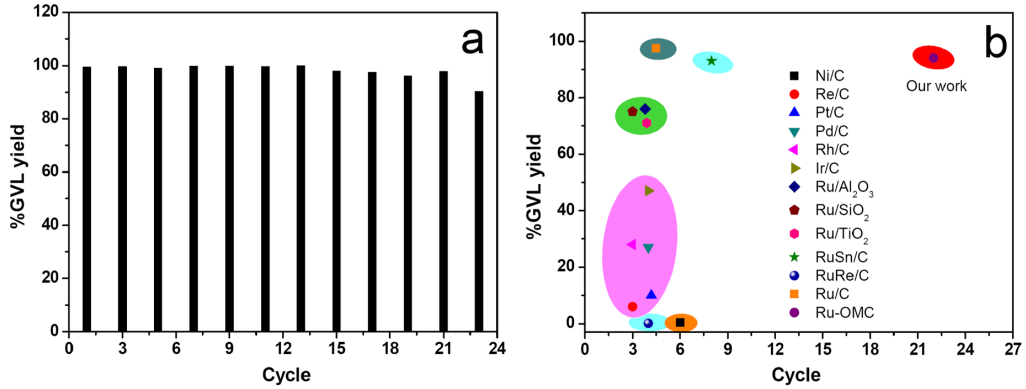

Figure 4 | Comparison of recycling over 3.0%Ru-OMC in this study (a) with various reported metal catalysts[4] (b) for LA hydrogenation. Reaction conditions: LA 5.0 g, catalyst amount 0.3 wt%, H_2 pressure 4.5 MPa, temperature 150°C and duration 2 h.

at 300°C for 3 h. The specific surface area was calculated using the Brunauer-Emmett-Teller (BET) method, and the pore size distributions were measured using the Barrett-Joyner-Halenda (BJH) method with the desorption branch of the isotherms. The synchrotron X-ray diffraction measurements were performed at the 11-ID-C beamline at the Advanced Photon Source (APS) at Argonne National Laboratory. High-energy X-rays (115 keV energy and 0.6 mm × 0.6 mm beam size) were used to obtain the two-dimensional (2D) diffraction patterns in transmission geometry with a Perkin-Elmer large area detector placed 1.6 m from the sample. The X-ray absorption fine structure (XAFS) was tested on beamlines20-ID and 20-BM at the APS at Argonne National Laboratory. The XAFS data were obtained in transmission mode at the Ru K-edge (22117.0 eV). The other related information and characterisation techniques can be found in Supplementary Information.

The metal content was estimated using inductively coupled plasma atomic emission spectroscopy (ICP-AES) conducted on a Perkin Elmer emission spectrometer. Each 10 mg sample was vacuum dried, placed in a digester with a PTFE lining, and dissolved in 5 ml of boiling aqua fortis solution. A microwave digestion was carried out for 10 min to dissolve the metal species completely. After cooling, each solution was filtered through a 0.45 μm polyethersulfone filter and then submitted to metal analysis.

1. Cerro-Alarcón, M., Maroto-Valiente, A., Rodríguez-Ramos, I. & Guerrero-Ruiz, A. Further insights into the Ru nanoparticles-carbon interactions and their role in the catalytic properties. *Carbon* **43**, 2711–2722 (2005).
2. Kubota, J. & Aika, K. Infrared studies of adsorbed dinitrogenon supported ruthenium catalysts for ammonia synthesis-effects of the alumina and magnesia supports and the cesium compound promoter. *J. Phys. Chem.* **98**, 11293–11300 (1994).
3. Xiong, K., Li, J. L., Liew, K. Y. & Zhan, X. D. Preparation and characterization of stable Ru nanoparticles embedded on the ordered mesoporous carbon material for applications in Fischer-Tropsch synthesis. *Appl. Cataly. A: Gen.* **389**, 173–178 (2010).
4. Wright, W. R. H. & Palkovits, R. Development of heterogeneous catalysts for the conversion of levulinic acid to γ-valerolactone. *ChemSusChem* **5**, 1657–1667 (2012).
5. Ruppert, A. M., Weinberg, K. & Palkovits, R. Hydrogenolysis goes bio: from carbohydrates andsugar alcohols to platform chemicals. *Angew. Chem. Int. Ed.* **51**, 2564–2601 (2012).
6. Van de Vyver, S., Geboers, J., Jacobs, P. A. & Sels, B. F. Recent advances in the catalytic conversion of cellulose. *ChemCatChem* **3**, 82–94 (2011).
7. Kobayashi, H., Komanoya, T., Hara, K. & Fukuoka, A. Water-tolerant mesoporous-carbon-supported ruthenium catalysts for the hydrolysis of cellulose to glucose. *ChemSusChem* **3**, 440–443 (2010).
8. Lee, J., Kim, J. J. & Hyeon, T. Recent progress in the synthesis of porous carbon materials. *Adv. Mater.* **18**, 2073–2094 (2006).
9. Pang, J. F. *et al*. Catalytic conversion of cellulose to hexitols with mesoporou scarbon supported Ni-based bimetallic catalysts. *Green Chem.* **14**, 614–617 (2012).
10. Xiong, K., Zhang, Y. H., Li, J. L. & Liew, K. Y. Catalytic properties of Ru nanoparticles embedded on ordered mesoporous carbon with different pore size in Fischer-Tropsch synthesis. *J. Energy Chem.* **22**, 560–566 (2013).
11. Yan, Z.-P., Lin, L. & Liu, S. J. Synthesis of γ-valerolactone by hydrogenation of biomass-derived levulinic acid over Ru/C catalyst. *Energy & Fuels* **23**, 3853–3858 (2009).
12. Galletti, A. M. R., Antonetti, C., Luise, V. D. & Martinelli, M. A. Sustainable process for the production of γ-valerolactone by hydrogenation of biomass-derived levulinic acid. *Green Chem.* **14**, 688–694 (2012).
13. Su, F. B. *et al.* Sandwiched ruthenium/carbon nanostructures for highly active heterogeneous hydrogenation. *Adv. Funct. Mater.* **17**, 1926–1931 (2007).
14. Liu, S.-H., Lu, R.-F., Huang, S.-J., Lo, A.-Y., Chien, S.-H. & Liu, S.-B. Controlled synthesis of highly dispersed platinum nanoparticles in ordered mesoporous carbons. *Chem. Commun.* 3435–3437 (2006).
15. Liu, S.-H. *et al.* Fabrication and characterization of well-dispersed and highly stable PtRu nanoparticles on carbon mesoporous material for applications in direct methanol fuel cell. *Chem. Mater.* **20**, 1622–1628 (2008).
16. Ma, S. Q., Goenaga, G. A., Call, A. V. & Liu, D.-J. Cobalt imidazolate framework as precursor for oxygen reduction reaction electrocatalysts. *Chem. Eur. J.* **17**, 2063–2067 (2011).
17. Afsahi, F., Vinh-Thang, H., Mikhailenko, S. & Kaliaguine, S. Electrocatalyst synthesized from metal organic frameworks. *J. Power Sources* **239**, 415–423(2013).
18. Ma, T.-Y., Liu, L. & Yuan, Z.-Y. Direct synthesis of ordered mesoporous carbons. *Chem. Soc. Rev.* **42**, 3977–4003 (2013).
19. Guibal, E. Heterogeneous catalysis on chitosan-based materials: a review. *Prog. Polym. Sci.* **30**, 71–109 (2005).
20. Liang, C. D., Li, Z. J. & Dai, S. Mesoporous carbon materials: synthesis and modification. *Angew. Chem. Int. Ed.* **47**, 3696–3717 (2008).
21. Wan, Y. & Zhao, D. Y. On the controllable soft-templating approach to mesoporous silicates. *Chem. Rev.* **107**, 2821–2860 (2007).
22. Viau, G. *et al.* Ruthenium nanoparticles: size, shape, and self-assemblies. *Chem. Mater.* **15**, 486–494 (2003).
23. Sarma, L. S. *et al.* Formation of Pt-Ru nanoparticles in ethylene glycol solution: an in situ X-ray absorption spectroscopy study. *Langmuir* **23**, 5802–5809 (2007).
24. Daniel, O. M. *et al.* X-ray absorption spectroscopy of bimetallic Pt-Re catalysts for hydrogenolysis of glycerol to propanediols. *ChemCatChem* **2**, 1107–1114 (2010).
25. Qiao, B. T. *et al.* Single-atom catalysis of CO oxidation using Pt_1/FeO_x. *Nat. Chem.* **3**, 634–641 (2011).
26. Zaikovskii, V. I. *et al.* Synthesis and structural characterization of Se-modified carbon-supported Ru nanoparticles for the oxygen reduction reaction. *J. Phys. Chem. B* **110**, 6881–6890 (2006).
27. Hwang, B. J. *et al.* Probing the formation mechanism and chemical states of carbon-supported Pt-Ru nanoparticles by in situ X-ray absorption spectroscopy. *J. Phys. Chem. B* **110**, 6475–6482 (2006).
28. Gallo, J. M. R., Pastore, H. O. & Schuchardt, U. Silylation of [Nb]-MCM-41 as an efficient tool to improve epoxidation activity and selectivity. *J. Catal.* **243**, 57–63 (2006).
29. Maurya, M. R. & Sikarwar, S. Oxidation of phenol and hydroquinone catalysed by copper(II) and oxovanadium(IV) complexes of N,N′-bis(salicyledene)diethylenetri-amine (H2saldien) covalently bonded to chloromethylated polystyrene. *J. Mol. Catal. A: Chem.* **263**, 175–185 (2007).
30. Maurya, M. R., Chandrakar, A. K. & Chand, S. Oxovanadium(IV) and copper(II) complexes of 1,2-diaminocyclohexane based ligand encapsulated in zeolite-Y for the catalytic oxidation of styrene, cyclohexene and cyclohexane. *J. Mol. Catal. A: Chem.* **270**, 225–235 (2007).
31. Zhang, F. Q. *et al.* A facile aqueous route to synthesize highly ordered mesoporous polymers and carbon frameworks with Ia3d bicontinuous cubic structure. *J. Am. Chem. Soc.* **127**, 13508–13509 (2005).
32. Hu, Q. Y. *et al.* Mesoporous carbon/silica nanocomposite through multi-component assembly. *Chem. Commun.* 601–603 (2007).
33. Liu, J. Y. Advanced electron microscopy of metal-support interactions in supported metal catalysts. *ChemCatChem* **3**, 934–948 (2011).
34. Zhang, B. *et al.* Electrochemical synthesis of catalytically active Ru/RuO_2 core-shell nanoparticles without stabilizer. *Chem. Mater.* **22**, 4045–4061 (2010).

Acknowledgments

PNC/XSD facilities at the Advanced Photon Source, and research at these facilities, are supported by the US Department of Energy - Basic Energy Sciences, a Major Resources Support grant from NSERC, the University of Washington, the Canadian Light Source and the Advanced Photon Source. Use of the Advanced Photon Source, an Office of Science User Facility operated for the U.S. Department of Energy (DOE) Office of Science by Argonne National Laboratory, was supported by the U.S. DOE under Contract No. DE-AC02-06CH11357. Financial supports for this research work from the National Natural Science Foundation of China (21303229), and Science Foundation of China University of Petroleum, Beijing (2462013YJRC018 and 2462013YJRC005) are also acknowledged.

Author contributions

Y.Y. performed the catalyst preparation, characterization and catalytic test, and wrote the paper. C.J.S. and Y.R. performed the XAFS and high-energy X-ray diffraction measurements. S.J.H. modified the paper. D.Q.J. helped in the HAADF measurement. All the authors discussed the results and commented on the manuscript.

Additional information

Supplementary information accompanies this paper at http://www.nature.com/scientificreports

Competing financial interests: The authors declare no competing financial interests.

How to cite this article: Yang, Y., Sun, C.J., Ren, Y., Hao, S.J. & Jiang, D.Q. New route toward building active ruthenium nanoparticles on ordered mesoporous carbons with extremely high stability. *Sci. Rep.* **4**, 4540; DOI:10.1038/srep04540 (2014).